COBEM 2023 27TH INTERNATIONAL CONGRESS OF MECHANICAL ENGENEERING

ABCM Brazilian Society of Mechanical Sciences and Engineering
27th ABCM International Congress of Mechanical Engineering
December 04-08, 2023, Florianópolis-SC, Brazil

COB-023-0077
AERODYNAMIC ANALYSIS OF TRUCK ACCESSORIES USING COMPUTATIONAL FLUID DYNAMICS

Leonardo Schultz
Diego Alves de Miranda
University of the Region of Joinville – UNIVILLE, Norberto Eduardo Weihermann, 230 - São Bento do Sul - SC.
leonardo.schultz@univille.br, diegoalves_klx@hotmail.com

Abstract: *Due to the growing need for road vehicles to have greater energy efficiency, a search was triggered not only for engines capable of greater and more economical yields, but also for accessories that contributed to the gain in truck aerodynamics, whether new or used. In this context, this study presents an aerodynamic analysis of different accessories that are attached to trucks in order to improve air flow around the vehicle. For this purpose, computer simulations of air flow in the Scania 440 model truck were used through the Ansys Fluent software. The condition of steady state and constant speeds were considered. The main objective was to measure the drag values for different usual traffic speeds, as well as the analysis of the behavior of the fluid around the body during contact. Based on the results, it was found among the analyzed accessories that the roof deflector demonstrated greater energy efficiency in road vehicles, being able to reduce fuel consumption by approximately 17% when compared to a truck without the use of deflectors.*
Keywords: *Aerodynamics, Energy Efficiency, Trucks, Drag Coefficient.*

1. INTRODUCTION

Faced with the constant relevance of road transport in the world, issues such as increasing the energy efficiency of these vehicles are increasingly being studied in various aspects. Because it is now understood that not only the powers offered, the resistance to body movements and the use of materials of less weight and greater resistance, but also the way in which the flow of fluid behaves along the body.

In the modal structure of cargo transport in Brazil, through the data survey carried out by EPE (2019), road transport is the most used, in relation to the others, representing approximately 59% of the total. The disadvantage of this mode of transport is the high cost, as fuel consumption is one of the most relevant factors.

According to (Bayindirli et al., 2016), the aerodynamics of the vehicle is directly related to its performance, so that it is responsible for ensuring the fluidity of the air around its contour and improving the conditions of forces such as drag and support generated. In addition to having to overcome the friction generated in the tires by the weight of the truck, as well as the trailer and the load, a considerable amount of fuel is consumed to overcome the drag and lift forces, which have their increase related to the gradual increase of the load.

Therefore, such forces must be reduced and result in an increase in the vehicle's mileage per liter of fuel. According to Pacheco and Miranda (2019), one of the ways to achieve this goal is to design vehicles with good geometries. In the case of this study then, it would generate an optimal relationship between the width and the radius of the edges of the truck, as well as the installation of skirts and air deflectors.

Different numerical methods have been used and suggested to reduce the drag force on land vehicles. Vaghela (2013) optimized the roof fairing angle of heavy trucks to reduce the drag force, using wind tunnel tests as validation. Chowdhury et al., (2013), conducted a series of numerical tests on a semi-trailer truck with different combinations of vehicle speed and yaw angles on a basic truck with various attachments. The results show an increase in the drag force for the yaw angle of up to 5°, subsequently there is a decrease in the drag force. Chilbule et al. (2014) performed numerical analyzes on a basic trailer truck model using ANSYS FLUENT. Just by modifying a wind deflector, the simulations showed a drag reduction of between 3% and 5%.

Within this context, this study sought to perform an analysis on the aerodynamics of a Scania 440 commercial cargo vehicle through CFD computational fluid dynamics, (Computational Fluid Dynamics) alternating aerodynamic devices designed to adapt these situations, in this case the air deflectors. Among the most relevant requirements is the reduction of the drag coefficient, which has a fundamental contribution to the vehicle's fuel consumption. The models were numerically simulated using the ANSYS Fluent software.

2. METHODOLOGY

The present work searches for accessories that can be used in the truck in order to reduce the aerodynamic drag. The modifications found will be compared with the original design, without any components, in order to measure the reduction in aerodynamic drag through comparative analysis.

2.1. Initial Study Parameters

Based on the research carried out, a list of accessories was generated, which will be evaluated separately, in order to find the contribution in reducing drag. This list is made up of two aerodynamic accessories that are highly widespread in vehicles, namely the roof deflector and the side deflector. To carry out the selection of equipment, the ease of installation of the accessories was taken into account and also the fact that they had already been tested in other studies.

To carry out a simplified analysis, trucks with a straight front and engine under the cabin were used, while the semi-trailer was analyzed for the box model. The equipment will be modeled based on those already tested in the work of Malin and Hakansson (2010), Hung and Davis (2009) and Wang et al. (2012).

2.2. Boundary Conditions

The tests will be simulated at 3 different speeds, 13.889 m/s, 19.44 m/s and 25 m/s (50 km/h, 70 km/h and 90 km/h), respectively. The choice of maximum speed is due to two reasons, initially, above 22.22 m/s, aerodynamic drag is the main factor responsible for the fuel consumption of the truck (MARLIM and HÅKANSSON, 2010). In addition, 25 m/s is the maximum speed limit allowed for trucks on single and double lane Brazilian highways (Brazilian Traffic Code Art. 61, 2021).

The simplified geometric model in CAD (Figure 1) becomes necessary due to the time and cost of analysis in CFD, which would be much greater if a complex geometry were used.

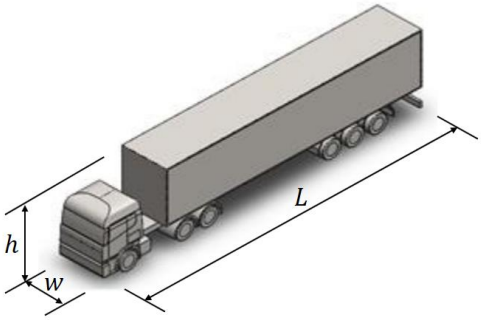

Figure 1. Simplified geometric model made in CAD.

Where L is the total length of the truck (m), w is the total width of the truck (m) and h is the total height of the truck (m).

2.3. Model Verification

The construction of the work is based on information obtained through simulations with commercial CFD software, Ansys. Therefore, to guarantee that the results will be the most reliable, that is, as close to reality as possible, it is necessary to guarantee that the conditions chosen to be simulated are correct.

For this, the validation by the method of the body of Ahmed was used. This method was developed by Ahmed (1983) and his research has been used as a validation parameter for CFD simulations, as he has several studies on this vehicle (Figure 2).

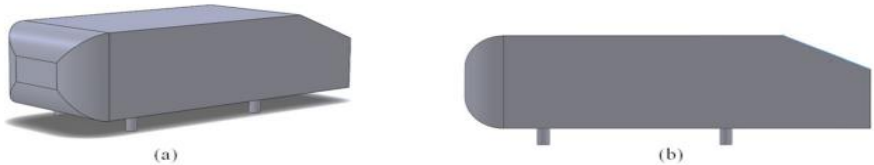

Figure 2. Ahmed's Body (1983). (a) Isometric view, (b) Side view. (Pacheco e Miranda, 2019).

If the simulation method produces results consistent with the results of several other authors in the model developed by Ahmed, Figure 2, there is a validation of the model where there are great chances of representing reality reliably. More details about this validation can be seen in the study by Pacheco and Miranda (2019).

2.4. Simulations

The aforementioned simulations and analyzes will be carried out using the CFD software (Fluent Ansys® 2020 R1). The Scania R440 model, LA 6x4 chassis, was used as geometry for the base truck, and as a wheel parameter, the RB662+R660 model, and the semi-trailer that will be used is a box type. They will be carried out with the same reference

model and with the same test procedure mentioned in the base articles, aiming to generate results for comparison. Therefore, it will be possible to measure the percentage of modification that a given accessory resulted in the global drag coefficient. Four different types of simulations shown in Figure 3 will be performed:

- Truck and semi-trailer without any aerodynamic accessories (three-dimensional simulation):
- Truck with integrated roof deflector (three-dimensional simulation);
- Truck with side deflector (three-dimensional simulation);
- Truck equipped with roof deflector and side deflector (three-dimensional simulation).

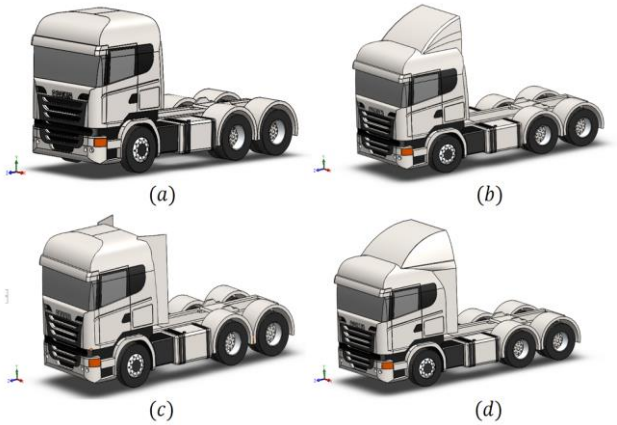

Figure 3. (a) CAD modeling of the truck without air deflectors; (b) CAD of truck with roof deflector; (c) CAD of truck with side deflector; (d) CAD of truck with two deflectors.

In order to carry out the simulations, it was necessary that the geometry was simplified in the wheels and also reduced to a scale of 1:32, in order to obtain a greater processing speed.

2.5. Drag Coefficient

To perform the drag calculation, the dimensionless drag coefficient is used, given by Equation 1:

$$Cd = \frac{F_d}{A\frac{\rho U^2}{2}} \tag{1}$$

Where C_d is the drag coefficient (adm), A is the reference area (m^2), U is the external velocity of the fluid (m/s), ρ is the specific mass of the fluid (kg/m^3) and F_d is the drag force (N). The drag coefficient is fundamental to determine the ease with which this body will move through the air, and reducing it is the objective to achieve greater efficiency (F1 TECHNICAL, 2006).

2.6. Pressure Coefficient

The pressure coefficient developed in Equation 2 characterizes the air flow pattern.

$$Cp = \frac{(P-P_\infty)}{P\infty\frac{U_\infty^2}{2}} \tag{2}$$

Where P is the local pressure, P_∞ is the external flow pressure (Pa) and U_∞ the free external flow velocity (m/s).

2.7. Navier-Stokes

Equation 3 represents the mass conservation equation, while equations 4, 5 and 6 represent the momentum conservation equations. All considering the incompressible fluid (FOX et al., 2009).

$$\frac{\partial u}{\partial x} + \frac{\partial v}{\partial y} + \frac{\partial w}{\partial z} = 0 \tag{3}$$

$$\rho\left[\frac{\partial u}{\partial t} + \frac{\partial u}{\partial x}u + \frac{\partial u}{\partial y}v + \frac{\partial u}{\partial z}w\right] = \frac{\partial p}{\partial x} + \mu\left(\frac{\partial^2 u}{\partial^2 x^2} + \frac{\partial^2 u}{\partial^2 y^2} + \frac{\partial^2 u}{\partial^2 z^2}\right) + \rho g(x) \tag{4}$$

$$\rho\left[\frac{\partial v}{\partial t}+\frac{\partial v}{\partial x}u+\frac{\partial v}{\partial y}v+\frac{\partial v}{\partial z}w\right]=\frac{\partial p}{\partial y}+\mu\left(\frac{\partial^2 v}{\partial^2 x^2}+\frac{\partial^2 v}{\partial^2 y^2}+\frac{\partial^2 v}{\partial^2 z^2}\right)+\rho g(y) \quad (5)$$

$$\rho\left[\frac{\partial w}{\partial t}+\frac{\partial w}{\partial x}u+\frac{\partial w}{\partial y}v+\frac{\partial w}{\partial z}w\right]=\frac{\partial p}{\partial z}+\mu\left(\frac{\partial^2 w}{\partial^2 x^2}+\frac{\partial^2 w}{\partial^2 y^2}+\frac{\partial^2 w}{\partial^2 z^2}\right)+\rho g(z) \quad (6)$$

The Navier-Stokes equations represent nonlinear partial differential equations that solve for the transport properties of fluid motion (velocity in the *u*, *v*, and *w* directions).

2.8. Turbulence Model

Narcizo and Miranda (2019) explain that the RANS (Reynolds Averaged Navier Stokes) model has as its main purpose the modeling and resolution of Equations 7 and 8, being efficient for qualitative analyzes of the aerodynamic performance of shape variations. This *k*-ε model uses two equations to describe the turbulent kinetic energy *k* and the turbulent kinetic energy dissipation ε.

$$\frac{\partial(\rho k)}{\partial t}+\vec{\nabla}(\rho k U)=\vec{\nabla}\left(\frac{\mu_t}{\sigma_k}\nabla K\right)+2\mu_t\,.\,S_{ij}\,.S_{ij}-\rho\varepsilon \quad (7)$$

$$\frac{\partial(\rho\varepsilon)}{\partial t}+\vec{\nabla}(\rho\varepsilon U)=\vec{\nabla}\left(\frac{\mu_t}{\sigma_\varepsilon}\nabla\varepsilon\right)+C_{1\varepsilon}\frac{\varepsilon}{k}\,2\mu_t\,.S_{ij}\,.S_{ij}-C_{2\varepsilon}\rho\frac{\varepsilon^2}{k} \quad (8)$$

Where *U* is the mean velocity vector, followed by μ_t the turbulent dynamic viscosity, σ_k the closure constant of the *k*-ω model, S_{ij} is the Reynolds tensor, σ_ε is the closure constant of the *k*-ε model, $C_1\varepsilon$ and $C_{2\varepsilon}$ are the closure constants of the *k*-ε RNG model.

2.9. Calculation of Fuel Consumption

To find out the percentage of variation in fuel consumption added to the use of simulated accessories, Equation 9 was used, which describes the method by Marlin and Håkansson (2010), which relates the reduction of the drag coefficient (ΔCd) and the reduced fuel consumption (FS):

$$FS\ (\%)=\Delta Cd\left(\frac{16}{30}\right) \quad (9)$$

2.10. Domain

In order to carry out the simulations, it was necessary to generate the geometry referring to the volume of the air flow that will come into contact with the surface of the designed vehicle. The closing function was used because it has good compatibility with the CFD software, as shown in Figure 4.

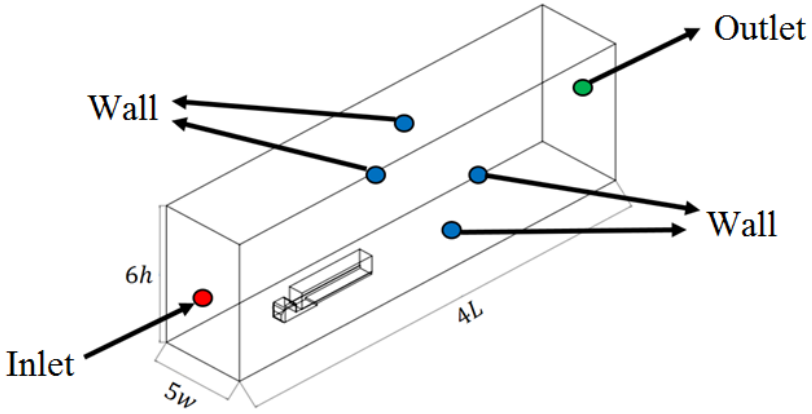

Figure 4. Geometry references generated for flow volume.

The domain must always have at least 4L, 5w and 6h, where L is the total length of the truck (m), w is the total width of the truck (m) and h is the total height of the truck (m). The mesh has great importance in validating the results.

3. RESULTS AND DISCUSSIONS

In this part of the work, the results of the fluid dynamic simulation carried out in the truck models will be approached and discussed.

3.1. Validation

The body method Ahmed (1983) was used to validate the simulations. Table 1 presents some drag and lift coefficient values abstracted from different fluid dynamic simulations applied to Ahmed's vehicle by some authors.

Table 1. Values of drag and lift coefficients abstracted by previous authors for S.R Ahmed's vehicle with a posterior angle of 25° and airflow velocity of 40 m s^{-1}.

Authors	***Cd***	***Cs***
Meile et al. (2011)	0.299	0.3450
Meile et al. (2016)	0.2964	0.358
Thacker et al. (2012)	0.3840	0.4220
Rossitto et al. (2016b)	0.356	0.311
Guilmeneau et al. (2017)	0.4371	0.3747
S. Krajnovic et al. (2017)	0.3718	0.3815
Pacheco e Miranda (2019)	0.3420	0.3730
Present Study (2023)	**0.3117**	**0.3698**

In this way, the values of the drag and lift coefficients of 0.3117 and 0.3698, respectively, were obtained. Which means that the method applied to the original object of study will provide results close to reality.

3.2. Mesh Convergence Analysis

One of the methods to verify the convergence of the model is the generation of meshes with different refinements, in order to compare the results. According to Figure 5, it can be seen that good mesh refinement requires good dimensioning and good inflation on the surface of the body.

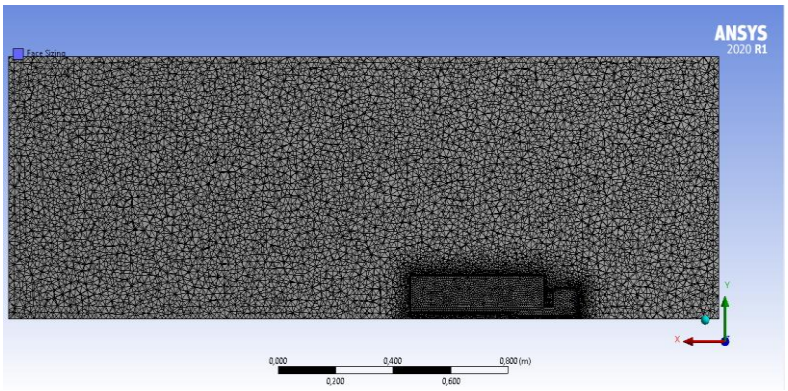

Figure 5. Refinement of the three-dimensional mesh (central section view).

3.3. Truck and Semitrailer Simulations Without Any Aerodynamic Accessories

The data presented will refer to a speed of 25 m/s (90 km/h), since at this speed drag will be the main responsible for the variation in fuel consumption. Table 2 shows the results for the test without any of the aerodynamic accessories.

Table 2. Results for the base truck.

Number of Elements	**Number of Nodes**	**Number of interactions until convergence**	***Cd***
789,263	163,916	965	0.82644

Figures 6 in (a), (b), (c) and (d) show respectively the velocity fluxes, the flux lines, the flux vectors, vehicle pressure field and temperature field.

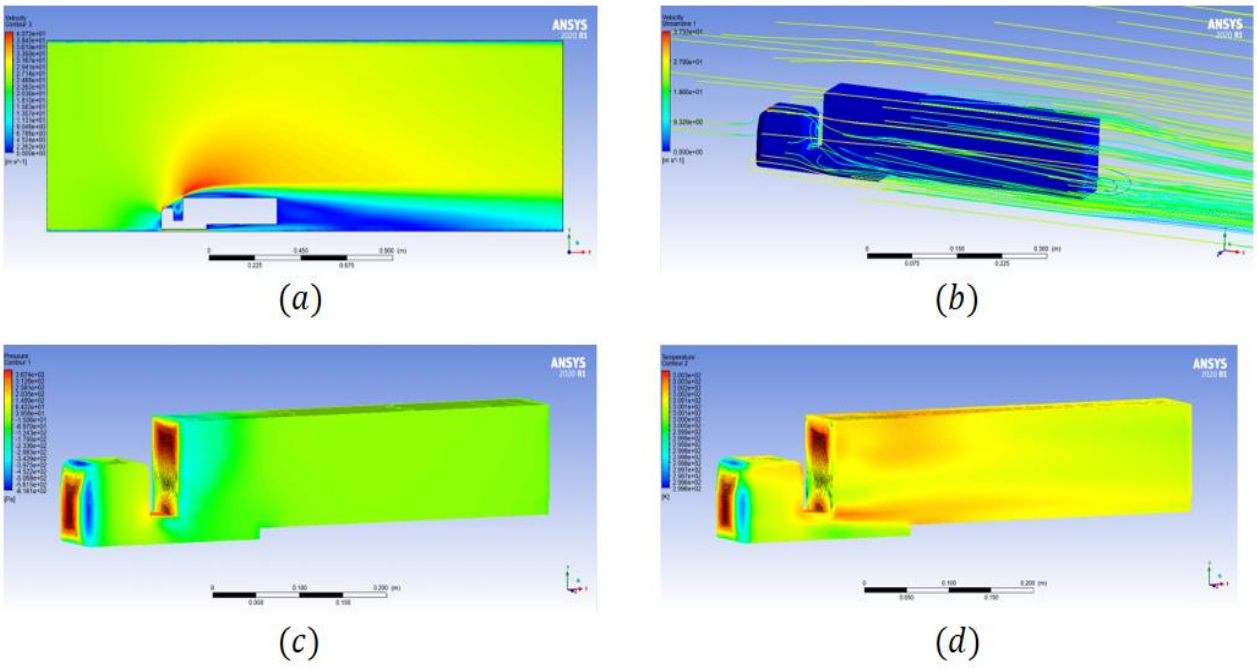

Figure 6. Base truck simulation results. (a). Flow lines side view (m/s). (b). Top view flow lines (m/s). (c). Pressure coefficient (Pa). (d). Temperature gradient (K).

To facilitate the identification of the scales, the same Figures of these simulations and the next ones, have been added in annex in enlarged size. Based on figures 6.a and 6.b, turbulent regions can be seen, in the range of 9m/s, on the upper and lower part of the truck and implement, as well as in the aerodynamic wake region of the semi-trailer. Turbulent regions are unstable and indicate large losses of flow energy that increase the aerodynamic drag coefficient (MARLIN and HAKANSSON, 2010).

Based on figure 6.c, note three regions of low pressure, varying between -400Pa and -200Pa, on the top and side of the truck and implement. In this case, due to the effect of flow acceleration on the circular geometry of the truck, a low pressure region is generated in this position. Since the low pressure region of the semi-trailer is the result of the collision of the flow with the straight face. On the other hand, there are high pressure points, located in the shock flow line (front of the truck and upper front part of the semi-trailer), which vary in the range of 300 Pa. In figure 6.d, it can be seen that the areas of highest pressure coincide with the areas of highest temperature.

3.4. Truck simulations with integrated roof deflector

Table 3 highlights the simulation parameters for the truck with roof deflector, as well as the Cd obtained.

Table 3. Result of the simulation with roof deflector.

Number of Elements	Number of Nodes	Number of interactions until convergence	*Cd*
883,542	120,019	950	0.55929

Figures 7 in (a), (b), (c) and (d) respectively show the velocity fluxes, the flux lines, the flux vectors, the vehicle's pressure field and the temperature field.

From the analysis of the velocity vectors, shown in Figures 7.(a) and 7.(b), it can be seen that the roof deflector acts in the region of greatest turbulence, which extends across the entire upper area of the semi-trailer , having great efficiency, to the point of transforming the flow from turbulent to laminar. Another observation that can be made in Figure 7.(b) is the behavior of the fluid flow located in the region between the truck and the semi-trailer. truck and its drainage ends at the top of the semi-trailer.

When analyzing Figure 7.(c), it is noticed that the low pressure region previously located on the upper part of the semi-trailer, in addition to ceasing to exist, generated a low pressure region in the space between the truck and the implement, points which also show an increase in temperature, as shown in Figure 7.(d).

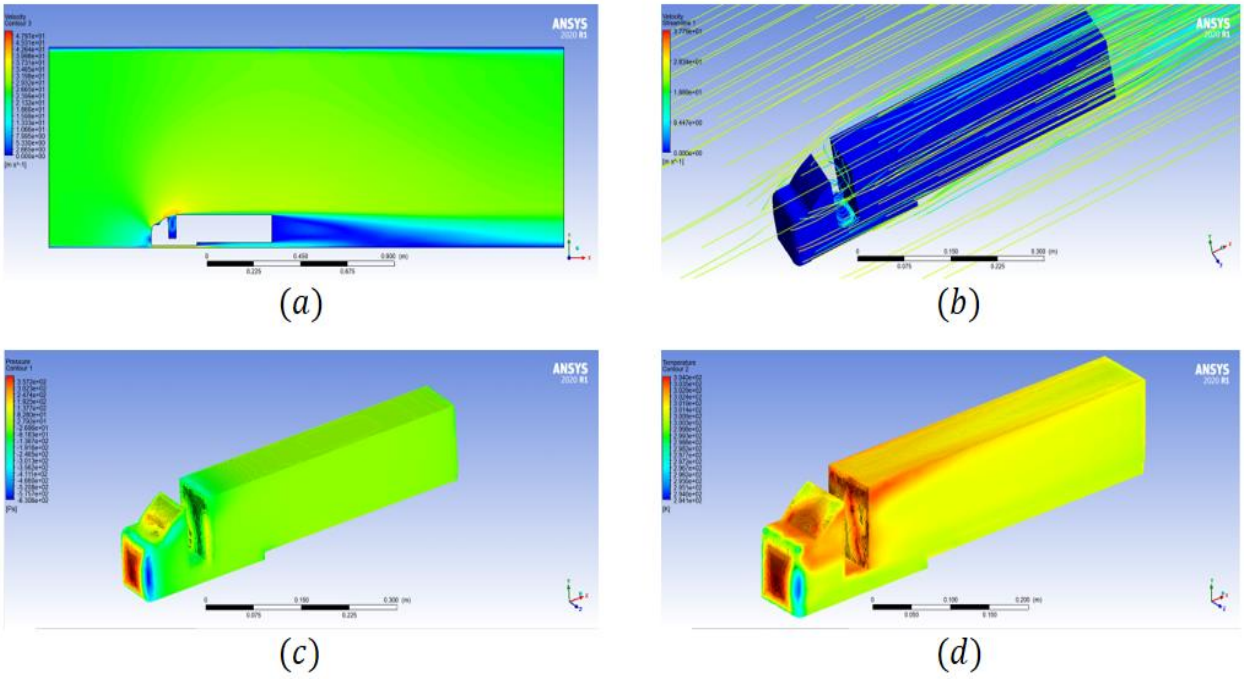

Figure 7. Results of simulations with integrated roof deflector. (a). Flow lines side view (m/s). (b). Top view flow lines (m/s). (c). Pressure coefficient (Pa). (d). Temperature gradient (K).

3.5. Base truck simulations with side deflector

The simulation parameters, as well as the *Cd* value obtained, can be seen in Table 4:

Table 4. Result of simulation with side deflector.

Number of Elements	Number of Nodes	Number of interactions until convergence	*Cd*
782,215	159,684	1,130	0.74858

Figures 8 in (a), (b), (c) and (d) show respectively the velocity flows, the flow lines, vehicle pressure field and temperature field.

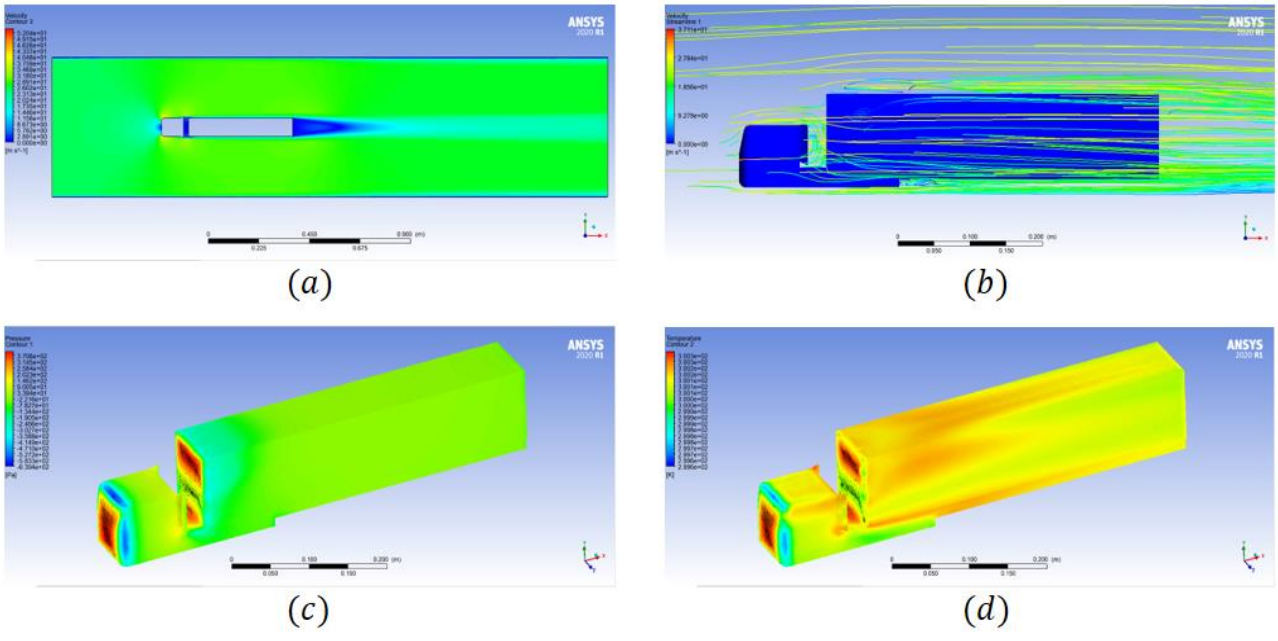

Figure 8. Results of simulations with lateral deflector. ((a). Flow lines side view (m/s). (b). Top view flow lines (m/s). (c). Pressure coefficient (Pa). (d). Temperature gradient (K).

Note that the side deflector has its functionality aimed at restricting the flow on the side of the truck, as can be seen in Figure 8.(a), in the range between 0 and 2 m/s, indicating low flow velocity in the space between the truck and the semi-trailer. While in Figure 8.(b) the flow of fluid is observed through the extension of the bodies, it is noted that the flow of fluid between the two bodies has less turbulence, in addition to having decreased the pressure and temperature in the same region, which leads to the reduction of *Cd*.

3.6. Base truck simulations with two deflectors

The simulation parameters, as well as the Cd value obtained, can be seen in Table 5:

Table 5. Result of simulation with front deflector.

Number of Elements	Number of Nodes	Number of interactions until convergence	*Cd*
798,859	167,086	520	0.48088

Figures 9 in (a), (b), (c) and (d) respectively show the flow lines (view 01), flow lines (view 02), vehicle pressure field and temperature field.

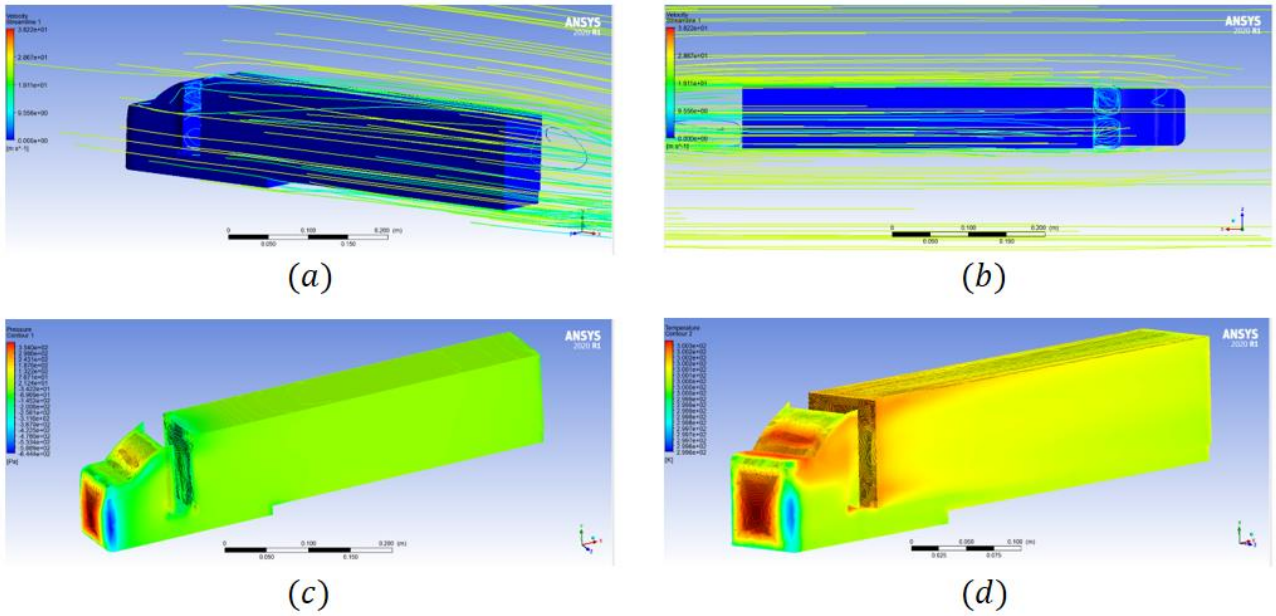

Figure 9. Results of simulations with lateral deflector. (a). Flow lines side view (m/s). (b). Top view flow lines (m/s). (c). Pressure coefficient (Pa). (d). Temperature gradient (K).

When comparing the results found for the base truck and for the trucks with both deflectors, the behavior of the fluid in the area between the two bodies (truck and semi-trailer) stands out. The fluid is much more controlled, in a laminar way, compared to the first results (Figure 6.(a) and 6.(b)), a fact which already characterizes a decrease in aerodynamic drag.

In Figure 8.(c), it can be seen that the pressure pattern is homogeneous at low and medium pressures (between -500Pa and -100Pa), with emphasis on the region between the bodies, which completely predominates at low pressures. Changes in the temperature aspect are also noted, demonstrating more moderate temperatures along the implement and areas of increased temperature between the two bodies.

3.7. Comparative analysis between aerodynamic accessories

To carry out the comparative analysis, the aerodynamic drag coefficients (*Cd*) obtained with the installation of each aerodynamic accessory were grouped, and compared with that found for the base truck (without any accessory) in order to measure which had the greatest efficiency in reducing of aerodynamic drag.

Table 6 shows the drag coefficient values obtained in the simulations, and next to each result, the percentage that each accessory reduced the aerodynamic drag value of the truck without deflectors.

Based on the results found, it is clear the great efficiency of using air deflectors in trucks in order to reduce aerodynamic drag. With emphasis on the roof deflector that showed the best results, second only to the union of both deflectors.

Table 6. *Cd* values of the accessories for the speed of 25 m/s.

Type	*Cd*	Reduction
Used base truck	0.82644	-
Truck with roof deflector	0.55929	32.32%
Truck with side deflector	0.74858	9.42%
Truck with two deflectors	0.48088	41.81%

It is worth mentioning that the use of these devices must be well dimensioned, otherwise it can cause the opposite effect of what was expected, increasing the aerodynamic drag of the truck. In this sense, the roof deflector showed great applicability in this function, since there are several models on the market, each one specifically sized for a certain truck and also for the type of load that it will carry, this data being of great relevance.

3.8. Evaluation of the reduction of fuel consumption

Using the calculated values of the percentage variation of the drag coefficient reduction, the percentage of reduction in fuel consumption can be calculated using Equation 9. The results for this stage of the work are shown in Table 7.

Table 7. Percent reduction in fuel consumption for a speed of 25 m/s.

Type	Consumption Reduction
Roof Deflector	17.23 %
Side Deflector	5.02 %
Roof Deflector + Side Deflector	22.3 %

Aerodynamic devices proved to be a valuable resource for companies, since even the equipment with the lowest performance studied in this work showed satisfactory results, which is why its great presence is seen in trucks. Together with the results, the importance of using roof deflectors was seen when used with some types of load, due to their great efficiency, with expressive results of 32.32% reduction in Cd and a reduction equivalent to 17.23% in consumption of fuel. When these two devices are put together, the results are even better, reaching a reduction in fuel equivalent to 22.3%.

4. CONCLUSIONS

The flow dynamics was used to approach the involved aspects, the same ones responsible for the reduction of the aerodynamic drag, characterizing which devices are more efficient. Regarding numerical modeling, the definition of a well-refined mesh and good simulation parameters proved to be important for the reliability of the results, reaching data close to reality.

It was concluded that the ceiling deflector has the highest energy efficiency among the studied devices. Emphasizing the situation generated, flat front truck, with motorization under the cabin and with a box-type semi-trailer. With the expected results having been achieved, in addition to all the knowledge acquired in the process, competence in the professional environment was thus guaranteed.

In order to complement this work, it is possible to simulate many other aerodynamic accessories available on the market for trucks and their implements. In addition to the creation of new equipment, increasingly enriching the national scenario of development and creation of new products.

5. REFERENCES

Ahmed, S.R. 1983. *Influence of Base Slant on the Wake Structure and Drag of Road Vehicles*. Journal of Fluids Engineering, v 105, n 4, p429-434.

Bayindirli, C., Akansu, Y., Salman, M.S. 2016. *The Determination of Aerodynamic Drag Coefficient Of Truck and Trailer Model By Wind Tunnel Tests*. International Journal of Automotive Engineering and Technologies, v. 5, n. 2, p. 53-60.

Chilbule, C., Upadhyay, A., Mukkamala, Y. 2014. *Analyzing the profile modification of truck-trailer to prune the aerodynamic drag and its repercussion on fuel consumption*. Procedia Engineering. v 97, n 1, p1208-1219.

Chowdhury, H., Moria, H., Ali, A., Khan, I., Alam, F., Watkins, S. 2013. *A study on aerodynamic drag of a semi-trailer truck*. Procedia Engineering. v 56, n 1, p201-205.

CÓDIGO TRÂNSITO. Disponível em: https://www.ctbdigital.com.br/artigo/art61#:~:text=Art.-,61,e%20as%20condi%C3%A7%C3%B5es%20de%20tr%C3%A2nsito. Acesso em 13/06/2021.

Empresa de Pesquisa Energética – EPE. *Transporte rodoviário de cargas: proposta para o reequilíbrio*. Acesso em 17/08/2021. Disponível em: http://www.epe.gov.br.

F1 TECHNICAL. *What is the drag coefficient in an F-1 car*? Disponível em: https://www.f1technical.net/forum/viewtopic.php?t=1861 Acesso em 13/06/2021.

Fox, R.W., Pritchard, P.J., McDonald, A.T. 2009. *Introdução à Mecânica dos Fluidos*. Rio de Janeiro, LTC Editora.

Guilmineau, E., Deng, G.B., Leroyer, A., Queutey, P., Visonneau, M., Wackers, J. 2017. *Assessment of hybrid RANS-LES formulations for flow simulation around the Ahmed body*. Computers & Fluids.

Hung, H.F., Davis, R. 2009. *Design Optimization of Tractor-Trailers for Drag Reduction. San Antonio*, Texas, 27th Applied Aerodynamics Conference.

Krajnovic, S., Minelli, G., Basara, B., Rao, A. 2018. *On the two flow states in the wake of a hatchback Ahmed body*. Journal of Wind Engineering & Industrial Aerodynamics. Gothenburg. v 173, p262-278.

Malin, J.L., Håkansson, C. 2010. *CFD Analysis of Aerodynamic Trailer Devices for Drag Reduction of Heavy Duty Trucks*. 77 pg. Master's Thesis in the Master's programme Automotive Engineering. Department of Applied Mechanics Division of Vehicle Engineering and Autonomous Systems CHALMERS UNIVERSITY OF TECHNOLOGY Göteborg, Sweden.

Meile, W., Brenn, G., Reppenhagen, A., Fuchs, A. 2011. *Experiments and numerical simulations on the aerodynamics of the Ahmed body*. CFD Lett. v 3, 3239, 2011.

Meile, W., Ladinek, T., Brenn, G., Reppenhagen, A., Fuchs, A. *Non symmetric bistable flow around the Ahmed body*. International Journal of Heat and Fluid Flow. v 57, n1, p34–47, 2016.

Narcizo, G.G., Miranda, D.A. 2019. *Numerical analysis of the air-fuel mixture in indirect and direct injection of four-stroke engines*. Revista de Engenharia Térmica, v.18, n.2, pp 89-97.

Pacheco, V.F., Miranda, D.A. 2019. *Aerodynamic Analysis of High Energy Efficiency Vehicles by Computational Fluid Dynamics Simulation*. Advanced Engineering Forum. Vol 32, pp 32-41.

Rossitto, G., Sicot, C., Ferrand, V., Boree, J., Harambat, F. 2016. *Influence of afterbody rounding on the pressure distribution over a fastback vehicle*. Experiments in Fluids. v 57, n 43.

Thacker, A., Aubrun, S., Leroy, A., Devinant, P. 2012. *Effects of suppressing the 3D separation on the rear slant on the flow structures around an Ahmed body*. Journal of Wind Engineering & Industrial Aerodynamics. v 107, p237–243.

Vaghela, K. 2013. *Optimization of Roof fairing angle to reduce the Aerodynamic Drag ofHeavy Duty Truck*. International Journal of Emerging Technologies in Computational and Applied Sciences. v 5, n 2, 9113-117.

Wang, X.Y., Xing, J.H., Lei, L., Teng, F.L. 2012. *Numerical Simulation to Investigate Influence of Additional Devices on Aerodynamic Drag for Heavy-Duty Commercial Truck*. Applied Mechanics and Materials, v 209, p2089-2093.

6. RESPONSIBILITY NOTICE

The authors are the only responsible for the printed material included in this paper.